Proc. of SPIE Conference on Biometric Technology for Human Identification III, (Orlando, USA), pp. 62020B-1 - 62020B-12, April 2006.

A Calibration Model For Fingerprint Sensor Interoperability

Arun Ross and Rohan Nadgir

West Virginia University, Morgantown, U.S.A

ABSTRACT

Biometric sensor interoperability refers to the ability of a system to compensate for the variability introduced in the biometric data of an individual due to the deployment of different sensors. We demonstrate that a simple non-linear calibration scheme, based on Thin Plate Splines (TPS), is sufficient to facilitate sensor interoperability in the context of fingerprints. In the proposed technique, the variation between the images acquired using two different sensors is modeled using non-linear distortions. Experiments indicate that the proposed calibration scheme can significantly improve inter-sensor matching performance.

Keywords: Fingerprint sensor interoperability; Fingerprint sensors; Calibration; Thin-plate splines (TPS); Inter-sensor distortion model; Average deformation.

1. INTRODUCTION

Fingerprints are oriented texture patterns consisting of ridges and valleys that are present on the tip of an individual's finger. Advances in sensor technology now permit the online acquisition of fingerprints using scanners based on optical, capacitive, piezoelectric, thermal or ultrasonic principles.[1] The sensing area of these scanners can vary from a few square millimeters to a few square inches. The resolution of the acquired image can vary anywhere between 250 dpi (e.g., Authentec's AF-S2 FingerLoc) and 512 dpi (e.g., Digital Persona's U.are.U 4000); scanners that acquire 1000 dpi images (e.g., Aprilis' HoloSensor) are also available in the market. The fingerprint images acquired using various sensing technologies may be significantly different. The inherent variation in the procured images is illustrated in Fig. 1, where five different scanners are used to capture impressions of the same fingerprint.

The variations introduced in the raw images due to differences in resolution, scanning area, sensing technology, etc. impact the features extracted from the images (e.g., minutiae points) and propagate into the stored templates. Most fingerprint matchers are restricted in their ability to compare fingerprints originating from two different sensors resulting in poor inter-sensor performance.[2] Inferior inter-sensor performance has been reported not only in the fingerprint domain but in other domains such as speech, iris and face as well. Martin et al.[3] report a significant drop in the matching performance of speech-based biometric systems when the input device is switched from a carbon-button microphone to a electret microphone (and vice versa). Results of the iris recognition test conducted by the International Biometric Group (IBG)[4] suggest that inter-sensor matching performance is lower than intra-sensor performance. In the face domain, the variations introduced due to different cameras is expected to affect the performance of face recognition algorithms as severely as variations introduced due to differing illumination patterns.[5]

The problem of sensor interoperability as defined in this paper cannot be solved by adopting a common biometric data exchange format.[6] Such a format merely aids in the *exchange* of feature sets between systems/vendors.[7] However, it does not provide a method to *compare* feature sets obtained from different sensors. The US-VISIT * program for example, obtains fingerprint (and face) information of certain travelers arriving at airports and seaports. A 500 dpi optical scanner with a sensing area of 1.2" $\times$ 1.2" is currently being used during the enrollment phase to procure fingerprint images. The introduction of a different sensor during the verification stage might render the current data unusable. The cost of re-enrolling individuals every time the

Further author information: (Send correspondence to Rohan Nadgir)
Arun Ross: E-mail: Arun.Ross@mail.wvu.edu, Telephone: 1 304 293 0405 ext 2556
Rohan Nadgir: E-mail: rnadgir@mix.wvu.edu, Telephone: 1 304 293 0405 ext 2539

*United States Visitor and Immigration Status Indicator Technology

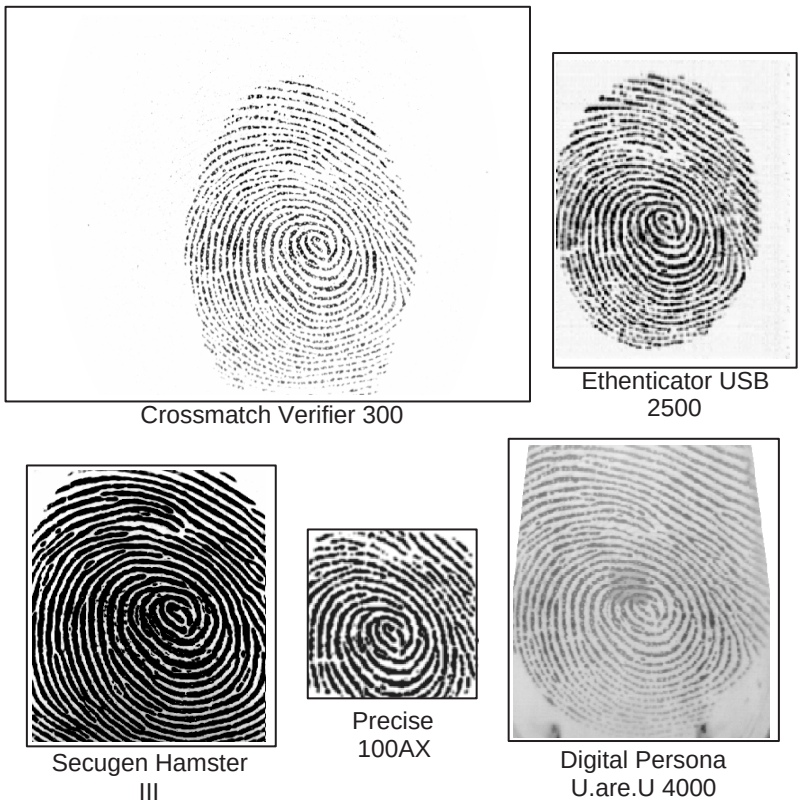

Figure 1. Observed differences between impressions of the same finger acquired using five different sensors. Verifier 300, Hamster III and U.are.U 4000 are optical sensors. Hamster III is based on SEIR (Surface Enhanced Irregular Reflection) technology, while U.are.U 4000 uses a FTIR (Frustrated Total Internal Reflection) technology. The USB 2500 is an electro-optical sensor and the 100AX is a capacitive sensor.

sensor is changed will be tremendous. In applications like these, the need for sensor interoperability is paramount and will significantly impact the usability of the system.

Besides changes in sensing technology, the fingerprint acquisition methodology may also vary across systems. Contact-based sensors can obtain rolled, flat, or slap prints of a finger (Fig. 2). The ability to successfully compare rolled prints against, for instance, the associated slap prints is indeed a challenging problem. This issue was highlighted in recent tests[8] involving FBI's IAFIS [†] (that uses 10 *rolled* prints) and INS' IDENT system [‡] (that uses two *flat* prints). Interoperability between these types of prints may entail the adoption of new matching algorithms and/or indexing schemes. In this work we concern ourselves with the interoperability between different sensing technologies (e.g., optical versus capacitive) and *not* between the modes of acquisition (e.g., rolled versus flat). In particular, we demonstrate that a simple non-linear calibration scheme is sufficient to facilitate sensor interoperability. In the proposed framework, the difference between the images acquired using two different sensors is modeled using non-linear distortions represented using Thin Plate Splines (TPS).

2. FINGERPRINT SENSING TECHNOLOGY

A brief overview of different fingerprint sensing technologies is provided in Table 1. The sensing technologies are categorized as Optical (FTIR and SEIR), Capacitive, Piezoelectric, Temperature Differential, Ultrasound, Touchless and Multispectral. Each sensing technology introduces its own distortions. Thus, deformation in

[†]Integrated Automated Fingerprint Identification System.

[‡]This is the fingerprint matching system used by DHS

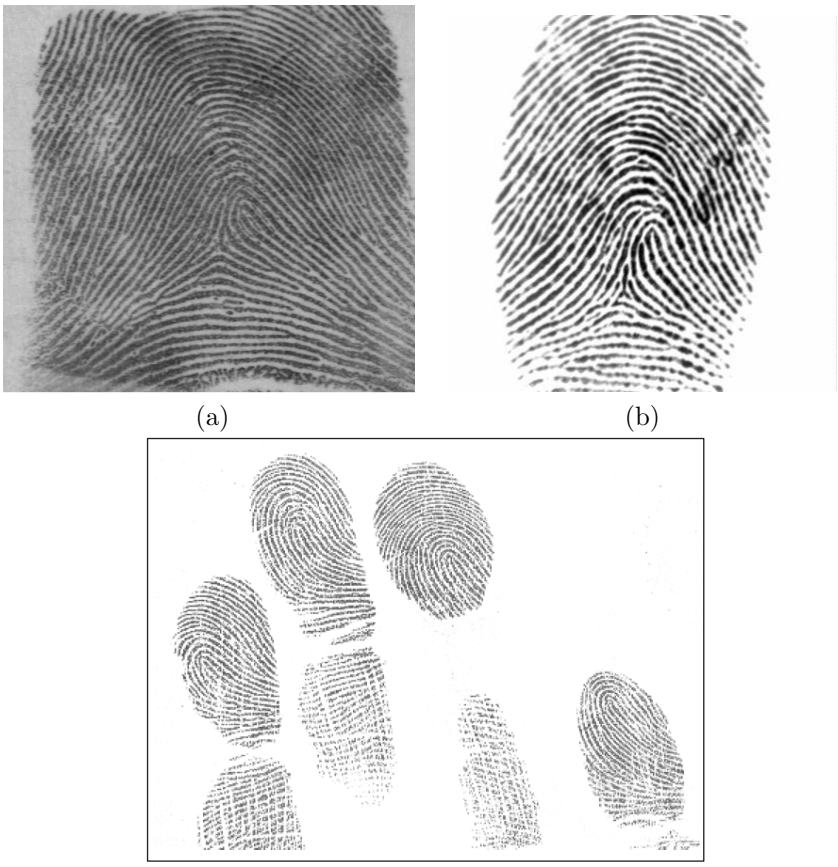

Figure 2. Fingerprint images obtained by different acquisition methodologies. (a) Rolled print (from the NIST Special Database 4); (b) Flat print (from the FVC 2002 DB1 Database); and (c) Slap print.[9]

fingerprint images is not only a consequence of the elastic nature of the skin during the image acquisition process, but the characteristic of the sensor itself. Distortions can occur in a fingerprint image when part of the image is either stretched, compressed or out of focus with respect to the rest of the image. Blurred edges are sometimes observed in images captured using optical scanners. This is due to the relatively larger size of the fingerprint area compared to the first lens in the lens assembly, leading to non-parallel light paths toward the edge of the image.[10] In some acquisition systems, the path lengths of reflected light differ across the length and width of the fingertip. Differences in path lengths can cause part of the image to be wider than the rest of the image - a principle known as Trapezoidal Distortion.[10–12] In Fig. 1, the image captured using Digital Persona's U.are.U 4000 exhibits this type of distortion. Varying path lengths also generate defocused areas within the captured image. The curvature of the lens assembly could lead to curved or out of focus appearance along the outer edges of the image. Capacitive sensors are prone to noisy artifacts, including noise from the 60 Hz power line and electrical noise from within the sensor. The semiconductor-sensing chips are also sensitive to electrostatic discharge, salt from sweat and other contaminants, as well as physical wear. Grid artifacts are possible in capacitive sensors. Hence, intrinsic sensor properties introduce distortions in the resulting images.

3. SENSOR INTEROPERABILITY

Biometric sensor interoperability refers to the ability of a system to compensate for the variability introduced in the biometric raw data of an individual due to the deployment of different sensors. In the context of fingerprints, interoperability may be addressed by two different approaches as shown in Fig. 3.

Table 1. Fingerprint Sensing Technologies.

No.	Sensing Technology	Working Principle	Products
1	Optical (FTIR - Frustrated Total Internal Reflection)	FTIR is based on total internal reflection. Light is reflected from valleys and not from ridges. Lens focuses the reflected light rays onto the camera. Valleys appear bright while ridges appear dark.[2, 10]	Digital Persona U.are.U 4000
2	Optical (SEIR - Surface Enhanced Irregular Reflection)	SEIR is based on scattering principles. Light is reflected and scattered from ridges and not from valleys. Most of the scattered light is collected, hence ridges appear bright while valleys appear dark.[10]	Secugen Hamster III
3	Capacitive	Air acts as dielectric medium. Capacitance is a function of distance of ridges and valleys from the capacitive plates.[2]	Fujitsu MBF200 Precise 100AX
4	Piezoelectric	Current is generated as a function of varying pressure applied by ridges and valleys on a dielectric material.[2]	Fidelica Microsystems FIS 3002
5	Temperature Differential	Current is generated as a function of varying temperature differentials observed across ridges and valleys.[2]	Atmel AT77C101B Sweeping sensor
6	Ultrasound	Image generated on basis of the response of the acoustic wave bounced off the fingertip. No skin contact.[2]	Ultra-Scan UltraTouch Model 203
7	Touchless	3-D image generated by integrating images captured by different cameras.†	TBS 3-D sensor. Surround Imaging(tm) technology
		Light reflected by ridges is converted into electrical signals to generate a image. Contact-less. ‡	TST group - BiRDIIi
8	Multispectral	Multispectral data is collected under different illumination angles and polarizing conditions as well as different wavelengths. Fingerprint information below the surface of the skin is captured easily.[13]	Lumidigm LightPrint Technology

(a) ***Distortion compensation model***: In this approach, the goal would be to determine and model the *physics* of the distortion process when a user places his finger on a particular scanner. This distortion would be based on the sensing technology of a particular scanner as well as the process employed to convert the sensed data into a raw image. As shown in Fig. 3(a), knowledge of the distortion process will permit us to compute the original "undistorted" fingerprint (canonical image). The canonical image may then be used for matching purposes.[14]

(b) ***Inter-sensor distortion model***: In the second approach, the *the relative distortion* between images acquired using two different sensors can be computed (Fig. 3(b)). Modeling the inter-sensor distortion may be viewed as a calibration problem, and can be accomplished by inheriting the knowledge of corresponding points on the two sensors. This is similar to the camera calibration problem which utilizes the knowledge of corresponding points on a chessboard plane for appropriate registration of two different cameras. The inter-sensor distortion will be a combination of affine as well as elastic distortions.

†`http://www.tbsinc.com/`

‡`http://www.tst-ag.de/`

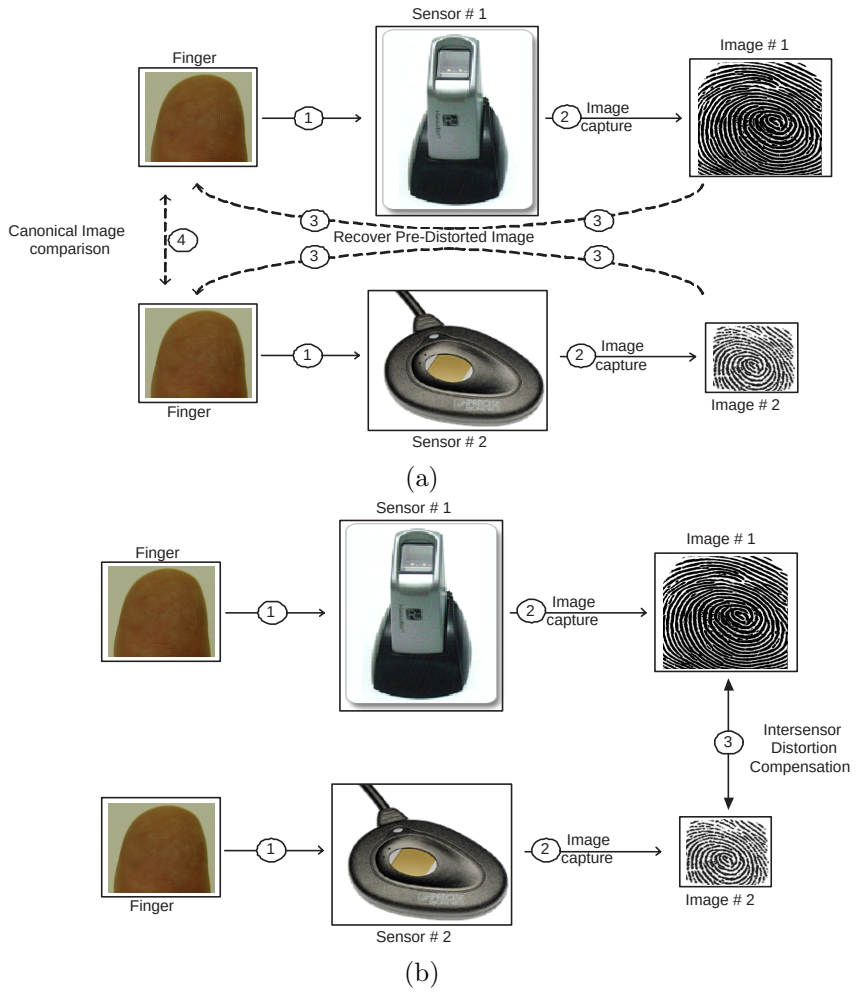

Figure 3. Two different ways of facilitating interoperability. (a) Distortion compensation model and (b) Inter-sensor distortion model. The numbers within circles denote the sequence of steps.

In this work, the second approach described above is used to address interoperability. A thin-plate spline (TPS) model is used to represent the inter-sensor distortion since it can account for the affine as well as the non-linear aspects of the deformation. The parameters of the inter-sensor distortion model rely on the evidence of control points present on the two sensors and their correspondence. In our approach, corresponding points (control points) are obtained by manually locating minutiae points from a *small* set of *representative* fingerprint image pairs (Fig. 4). The control points are selected manually to approximately cover the whole area within the smaller fingerprint image in order to model the distortions occurring in different areas of the representative image. These control points are then used to derive a deformation that represents the relative distortion between the two images (Fig. 5). Procrustes analysis of the control points assists in the removal of translation and rotation effects. The TPS model is used to compute the affine and the non-linear parameters from the modified control points. These parameters are computed for several representative image pairs based on the manually established control points. Multiple sets of TPS parameters aid in generating an average deformation model,[15] which defines the perturbation at every pixel (point) on one sensor with respect to the other.

The resulting average deformation model may be used for minutiae as well as image calibration. In minutiae calibration, the new minutia location of one image is calculated by perturbing the original minutia location based on the average deformation model. The calibrated minutiae set is then used for matching purposes. In image

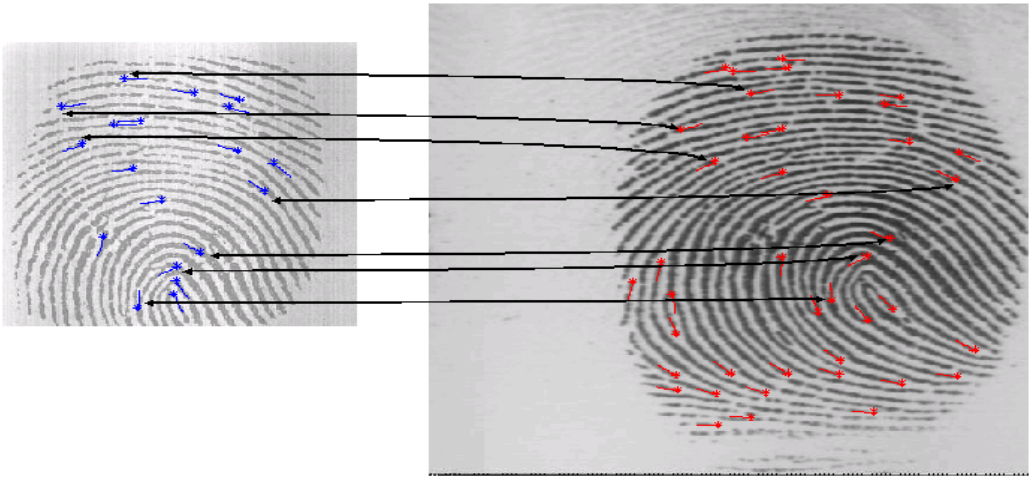

Figure 4. Minutiae correspondence (manually selected) across representative image pairs, serve as inputs to the TPS model.

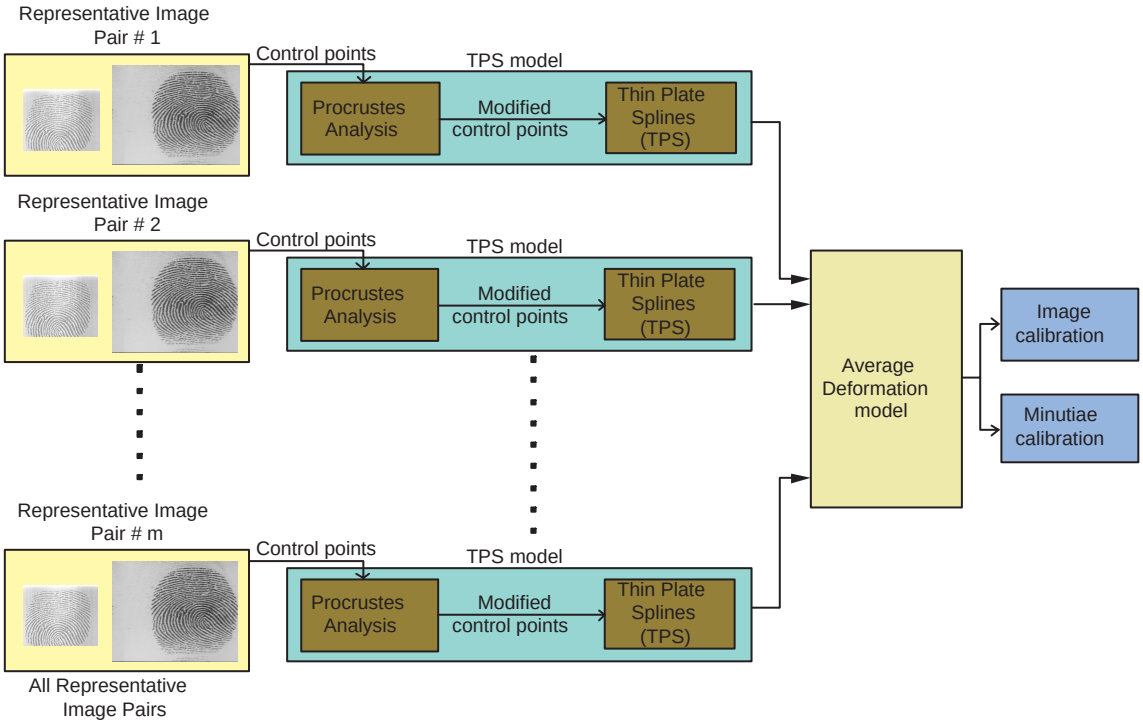

Figure 5. Manually selected control points from representative image pairs are provided as inputs to the TPS model. The affine and non-linear parameters derived from the average deformation model are used for image and minutiae calibration during the authentication stage.

calibration, the original fingerprint image is subjected to the transformation defined by the average deformation. Minutiae are then extracted from this calibrated image and later utilized during the matching stage.

The inter-sensor distortion model can be incorporated into a minutiae-based matcher for successful comparison of templates originating from different sensors (Fig. 6).

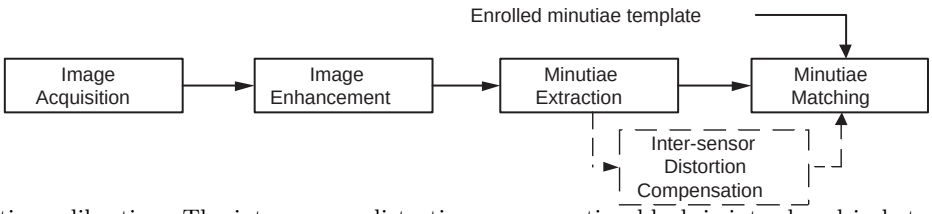

Figure 6. Minutiae calibration: The inter-sensor distortion compensation block is introduced in-between the minutiae extraction and matching modules to handle inter-sensor distortions.

4. THIN PLATE SPLINE MODEL

For spatial rearrangement of points, thin-plate spline (TPS) succinctly expresses the dependence of the physical bending energy of a thin metal plate on point constraints.[16] Recently, TPS has been used to model the non-linear deformations in fingerprints.[15, 17, 18] Given a list of corresponding points between the k^{th} representative image pair, the TPS function, F_k, calculates the transformed co-ordinates (u', v') as a function of the original co-ordinates (u, v). The TPS model interpolates the corresponding grid points while maintaining smoothness as defined by the bending energy of the thin metal plate. Here, the (u, v) points are in sensor 1 and the (u', v') points are the corresponding points in sensor 2. The function F_k is defined for each pixel (u, v) on sensor 1 and can be written as

$$(u', v') = F_k(u, v) = \begin{bmatrix} h_{1u} \\ h_{1v} \end{bmatrix} + \begin{bmatrix} h_{2u} \\ h_{2v} \end{bmatrix} u + \begin{bmatrix} h_{3u} \\ h_{3v} \end{bmatrix} v + \sum_{i=1}^{n} \begin{bmatrix} w_{iu} \\ w_{iv} \end{bmatrix} U(|G_i - (u, v)|), \quad (1)$$

where $U(r) = r^2 log(r^2)$ is the basis function, the h_1's, h_2's, h_3's are the parameters of the affine transformation, w_i's represent the weights for the non-linear transformation, $|.|$ is the L_2 norm and G_i, $i = 1..n$, are the control points corresponding to sensor 1. The affine parameters and the non-linear weights can be derived in a closed form solution according to the bending energy constraint which minimizes the curvature at every point in the grid (refer to Appendix A for the derivation). The *average* deformation of an arbitrary pixel (u, v) on sensor 1, denoted by $\overline{F}(u, v)$, is computed from the m TPS functions, $F_1, F_2, \ldots, F_m$ as

$$\overline{F}(u, v) = \sum_{k=1}^{m} \frac{F_k(u, v)}{m}. \quad (2)$$

5. RESULTS

In order to test the efficacy of the proposed calibration model, we use the MSU dataset comprising of fingerprint images obtained using two different sensor technologies: an optical Digital Biometrics (DBI) sensor and a solid-state capacitive VERIDICOM (VERI) sensor.[19] The 500 dpi DBI sensor has a platen area of 1" × 1" and acquires images of size 480 × 508. The 500 dpi VERI sensor has a sensing area of 0.6" × 0.6" and results in images of size 300 × 300. A sample image from each sensor is shown in Fig. 7. We observe that the two images, although obtained using sensors of similar resolution, have very different spatial characteristics.

Data from 128 different non-habituated cooperative subjects was available ¶. All subjects provided 4 images each of 4 distinct fingers for both the scanners. Thus, 4 impressions each of 512 different fingers were available. Two different minutiae-based matchers, the BOZORTH3 matcher developed by NIST and the VeriFinger matcher developed by Neurotechnologija were used in our experiments. The calibration model was computed using 8 different representative image pairs obtained from the two sensors. In our experiments, the VERI sensor was calibrated with respect to the DBI sensor. The mesh-grid plot of the original VERI image and the calibrated image (using average deformation) is shown in Fig. 8.

¶Although data from more number of users was available, only 128 of these users had data pertaining to both the sensors

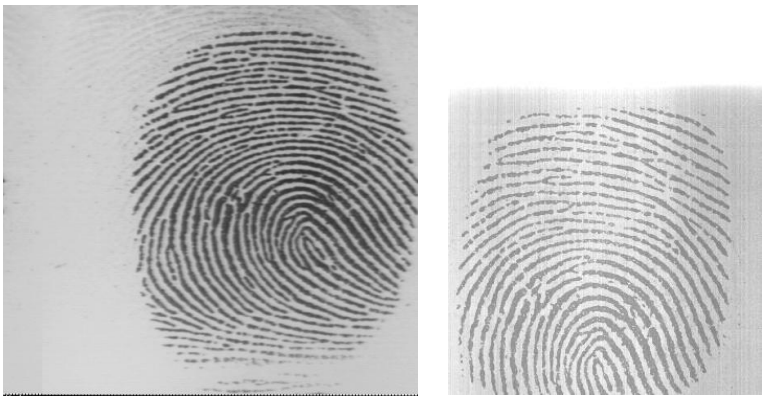

(a) (b)

Figure 7. Sample fingerprints from Digital Biometrics (DBI) and VERIDICOM (VERI) sensors. (a) Image acquired from DBI. (b) Image acquired from VERI.

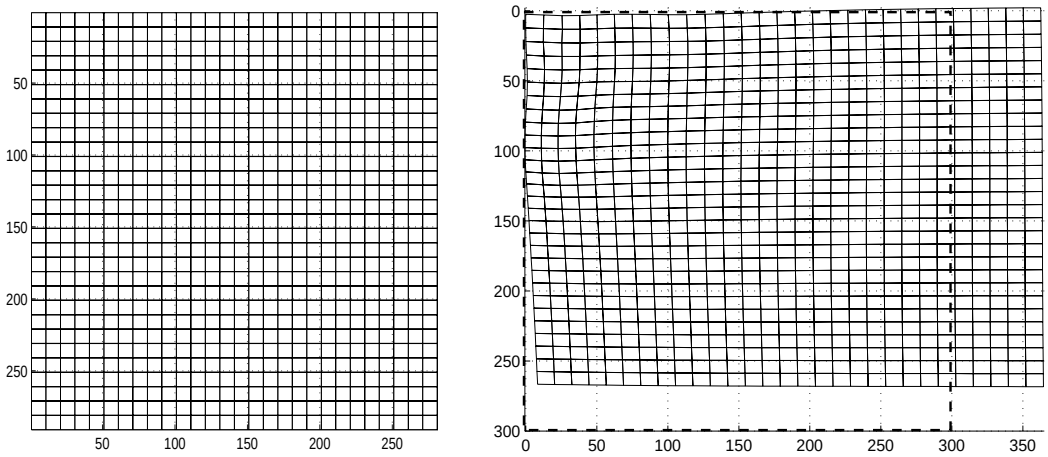

(a) (b)

Figure 8. Mesh-grid plot constructed using the parameters derived from the calibration model. (a) Original mesh-grid plot of VERI. (b) Calibrated mesh-grid plot after applying the average deformation. The dashed rectangle in (b) represents the original dimensions of the image.

Five different matching experiments were conducted using each of the two matchers in order to demonstrate the benefit of the calibration model:
(a) DBI vs DBI : The genuine and impostor match scores were generated by comparing minutiae sets within the DBI database.
(b) VERI vs VERI : The genuine and impostor match scores were generated by comparing minutiae sets within the VERI database.
(c) VERI vs DBI (before calibration): The genuine and impostor match scores were generated by comparing the VERI minutiae sets with the DBI minutiae sets.
(d) VERI vs DBI (after minutiae calibration): The minutiae sets extracted from the VERI images were subjected to the average deformation computed using our calibration model before matching them against the minutiae sets of the DBI images. An illustration of the original minutiae set of a VERI image along with the calibrated minutiae is provided in Fig. 9 (a & b).
(e) VERI vs DBI (after image calibration): The calibration model suggested here was also used to distort the images acquired using the VERI scanner before extracting the minutiae from them. However, the application of

a non-linear transformation to individual image pixels will generate sub-pixel information which can confound the minutiae detection process. One way to address this issue would be to subject the image to a simple affine transformation (predominantly scaling along the X- and Y- directions) before extracting minutiae points. These scaling factors were calculated as the average of the corresponding affine parameters computed by the calibration model based on the 8 representative image pairs. The mesh grid plots along with the minutiae obtained after image calibration are shown in Fig. 9 (c). As the minutiae are extracted from the images obtained after calibration, the minutiae count might be altered.

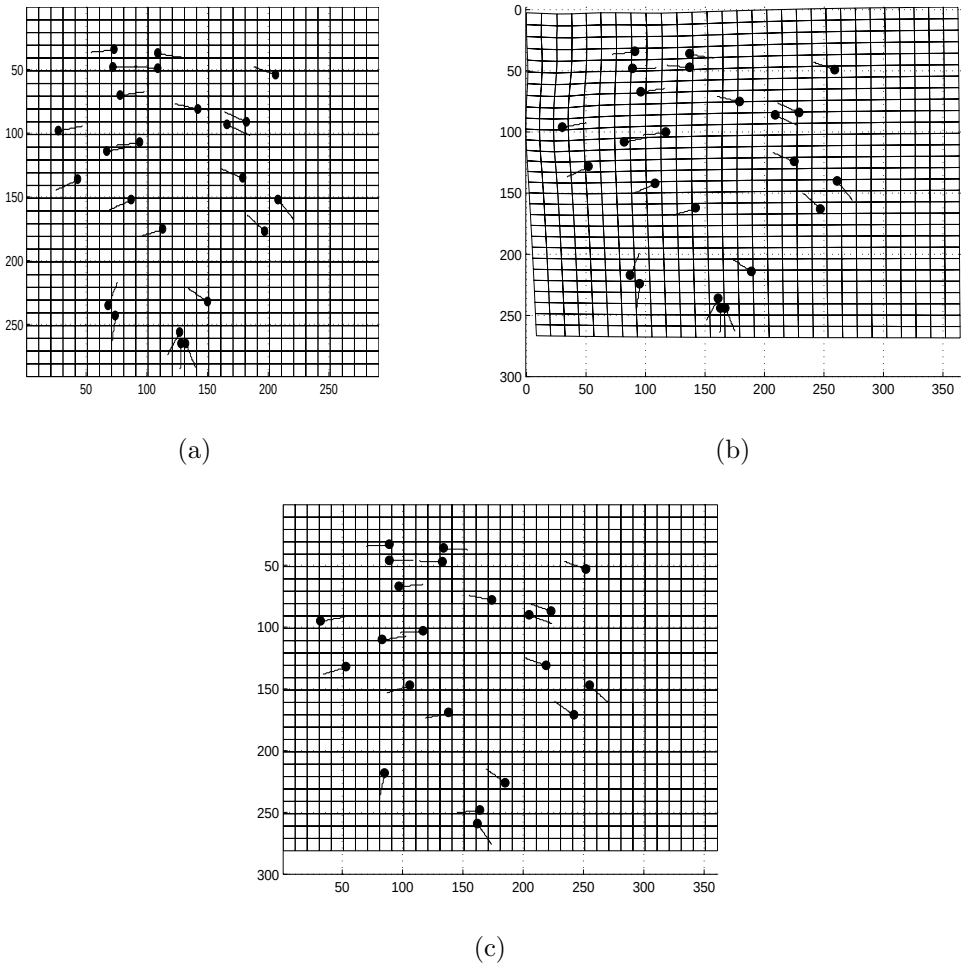

Figure 9. (a) Original mesh-grid plot with minutiae (b) Mesh-grid plot with calibrated minutiae (after minutiae calibration) (c) Mesh-grid plot with minutiae (after image calibration)

The Receiver Operating Characteristic (ROC) curves summarizing the performance of these 5 experiments using both the matchers is shown in Fig. 10. It is observed that the proposed calibration model results in improved inter-sensor matching performance. For example, in the scenario involving VERI vs DBI (after minutiae calibration) the GAR (Genuine Accept Rate) is observed to increase from $\sim 30\%$ to $\sim 70\%$ at a FAR (False Accept Rate) of 0.01% when the VeriFinger matcher is used,. Similarly, when the BOZORTH3 matcher is used, the GAR increases from $\sim 35\%$ to $\sim 65\%$ at the same FAR. Similar observations can be made in the case of image calibration. Thus, we state that a simple non-linear calibration scheme is sufficient to address the problem of interoperability. This, however, does not undermine the development of sophisticated matching algorithms that

utilize information such as ridge counts between minutiae points when comparing minutiae sets pertaining to multiple sensors. Such approaches have their own merits since they would preclude the establishment of manual correspondences. In minutiae calibration, the current formulation only perturbs the location of individual minutia points; it does not recompute the orientations of the minutiae points based on the non-linear calibration scheme. By changing the orientation appropriately, the inter-sensor performance, after minutiae calibration, may be further improved. However, this has not been tested as yet.

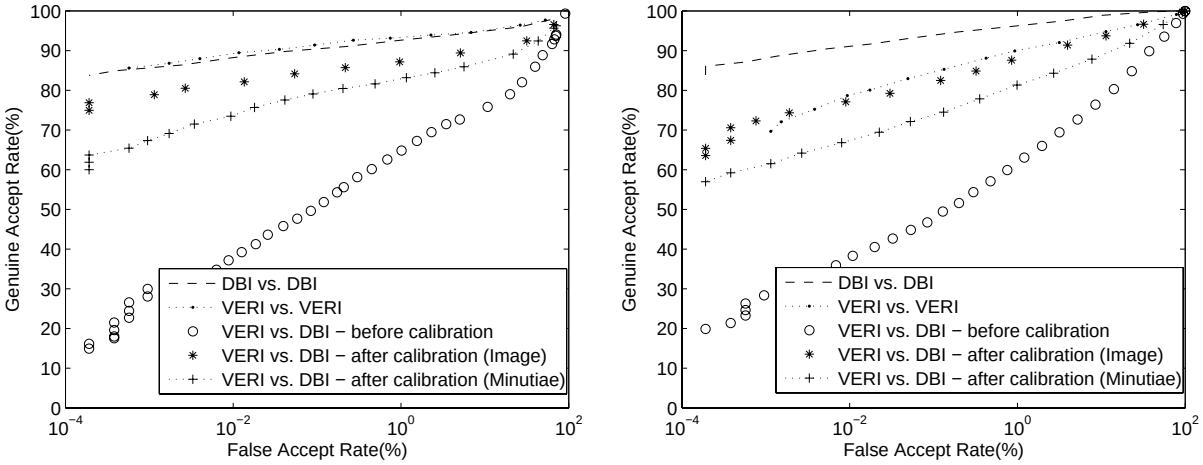

Figure 10. ROC curves indicating the improvement in inter-sensor performance on the MSU database. (a) VeriFinger matcher. (b) BOZORTH3 matcher.

6. SUMMARY AND FUTURE WORK

In this paper we have demonstrated that a simple non-linear calibration scheme based on TPS is sufficient to handle variations in minutiae distributions across multiple sensors. The parameters of the model (average deformation) are computed based on a small representative set of image pairs having control points whose correspondences are manually established. The average deformation is used to distort the minutiae points of images acquired using one sensor before comparing them with the minutiae points of images corresponding to another sensor. A significant performance improvement is observed when the proposed scheme is utilized to compare fingerprint images originating from two different sensors, viz., optical and solid state capacitive sensors. Only a few representative image pairs are needed for the successful implementation of the proposed method. In future, we plan to use more sophisticated calibration grids (similar to camera calibration in computer vision) by imaging rigid finger-like synthetic material with pre-established control points. This would avoid issues related to the elasticity of the skin.

Currently, we are acquiring data from 4 different sensors (Crossmatch Verifier 300, Ethenticator USB 2500, Secugen Hamster III, Precise 100 AX) in order to study the interoperability issues associated with them. A generic calibration model, based on automated control point selection from the representative image pairs, is essential to facilitate interoperability across a wide range of sensors. We are also developing alternate fingerprint matching schemes to address interoperability between minutiae sets obtained from multiple sensors. We plan to extend our approach toward addressing compatibility between slap and rolled prints.

ACKNOWLEDGMENTS

This project was funded by the Center for Identification Technology Research (CITeR) at West Virginia University. We are grateful to Dr. Stephanie Schuckers and Dr. Sunil Kumar of Clarkson University for their insightful comments. We would like to thank Dr. Anil Jain of Michigan State University for granting us access to the MSU Fingerprint Database.

APPENDIX A. THIN PLATE SPLINE PARAMETERS

The following derivation is based on Bookstein[16]. Let $G_1 = (u_1, v_1)$, $G_2 = (u_2, v_2)$, $\cdots$, $G_n = (u_n, v_n)$ be the control points in sensor 1 and $G'_1 = (u'_1, v'_1)$, $G'_2 = (u'_2, v'_2)$, $\cdots$, $G'_n = (u'_n, v'_n)$ be the corresponding control points in sensor 2. The basis function is given by $U(r_{ij}) = r_{ij}^2 log(r_{ij}^2)$, where $r_{ij} = |G_i - G_j|$. Then matrices K and P can be defined as,

$$\mathbf{K} = \begin{bmatrix} 0 & U(r_{12}) & \cdots & U(r_{1n}) \\ U(r_{21}) & 0 & \cdots & U(r_{2n}) \\ \cdots & \cdots & \cdots & \cdots \\ U(r_{n1}) & U(r_{n2}) & \cdots & 0 \end{bmatrix}_{n \times n};$$

$$\mathbf{P} = \begin{bmatrix} 1 & u_1 & v_1 \\ 1 & u_2 & v_2 \\ \cdots & \cdots & \cdots \\ 1 & u_n & v_n \end{bmatrix}_{n \times 3}.$$

Let ^{T} be the matrix transpose operator and O be a 3×3 matrix of zeros, then L is given as

$$\mathbf{L} = \left[\begin{array}{c|c} K & P \\ \hline P^T & O \end{array}\right]_{(n+3)\times(n+3)}.$$

Define Y as

$$\mathbf{Y} = \left[\begin{array}{cccc|ccc} u'_1 & u'_2 & \cdots & u'_n & 0 & 0 & 0 \\ v'_1 & v'_2 & \cdots & v'_n & 0 & 0 & 0 \end{array}\right]_{2\times(n+3)}.$$

The affine and non-linear deformation parameters can be estimated as,

$$L^{-1}Y^T = (W|h)^T$$

where,

$$\mathbf{W} = \begin{bmatrix} w_{1u} & w_{2u} & \cdots & w_{nu} \\ w_{1v} & w_{2v} & \cdots & w_{nv} \end{bmatrix}_{2\times n};$$

$$h = \begin{bmatrix} h_{1u} & h_{2u} & h_{2u} \\ h_{1v} & h_{2v} & h_{2v} \end{bmatrix}_{2\times 3}.$$

This gives us the M matrix,

$$\mathbf{M} = \left[\begin{array}{ccc|cccc} h_{1u} & h_{2u} & h_{3u} & w_{1u} & w_{2u} & \cdots & w_{nu} \\ h_{1v} & h_{2v} & h_{3v} & w_{1v} & w_{2v} & \cdots & w_{nv} \end{array}\right]$$

where, the h_{ij}'s represent the affine parameters and w_{ij}'s represent the non-linear deformation parameters.

REFERENCES

1. D. Maltoni, D. Maio, A. K. Jain, and S. Prabhakar, *Handbook of Fingerprint Recognition*, Springer, July 2003.
2. A. Ross and A. Jain, "Biometric sensor interoperability: A case study in fingerprints," in *Proc. of International ECCV Workshop on Biometric Authentication (BioAW)*, **LNCS**, pp. 134–145, May 2004.
3. A. Martin, M. Przybocki, G. Doddington, and D. Reynolds, "The NIST speaker recognition evaluation - overview, methodology, systems, results, perspectives (1998)," *Speech Communications* **31**, pp. 225–254, 2000.

4. International Biometric Group, "Independent testing of iris recognition technology (ITIRT) - Final Report," May 2005.
5. P. J. Phillips, A. Martin, C. l. Wilson, and M. Przybocki, "An introduction to evaluating biometric systems," *IEEE Computer Society* **33**, pp. 56–63, February 2000.
6. F. Podio, J. Dunn, L. Reinert, C. Tilton, L. OGorman, P. Collier, M. Jerde, and B. Wirtz, "Common biometric exchange file format (CBEFF)," NIST Interagency Report 6529, NIST, 1999.
7. R. M. Bolle, N. K. Ratha, A. Senior, and S. Pankanti, "Minutia template exchange format," in *Proc. of IEEE Workshop on Automatic Identification Advanced Technologies*, pp. 74–77, (Summit, NJ), 1999.
8. A. Hicklin and C. Reedy, "Implications of IDENT/IAFIS image quality study for visa fingerprint processing," tech. rep., Mitretek Systems, October 2002.
9. B. Ulery, A. Hicklin, C. Watson, M. Indovina, and K. Kwong, "Slap fingerprint segmentation evaluation 2004," NIST Interagency Report 7209, NIST and Mitretek Systems, March 2005.
10. Secugen Biometric Solutions, "SEIR optic technology," White Paper, Secugen, 2004. (Available at `http://www.secugen.com/company/ip.htm`).
11. H. H. Teng and S.-C. Jo, "Method and apparatus for reduction of trapezoidal distortion and improvement of image sharpness in an optical image capturing system." US Patent 6,324,020 B1, November 27 2001.
12. H. H. Teng and S.-C. Jo, "High contrast, low distortion optical acquisition system for image capturing." US Patent 6,381,347 B1, April 30 2002.
13. M. S. Ennis, R. K. Rowe, S. P. Corcoran, and K. A. Nixon, "Multispectral sensing for high-performance fingerprint biometric imaging," White Paper, Lumidigm Inc. (Available at `http://www.lumidigm.com/lightPrint.html`).
14. A. Senior and R. Bolle, "Improved fingerprint matching by distortion removal," *IEICE Transactions on Information and Systems* **E84-D**, pp. 825–831, 2001.
15. A. Ross, S. Dass, and A. Jain, "A deformable model for fingerprint matching," *Pattern Recognition* **38**, pp. 95–103, January 2005.
16. F. L. Bookstein, "Principal warps: Thin-plate splines and the decomposition of deformations," *IEEE Transactions on Pattern Analysis and Machine Intelligence* **11**, pp. 567–585, June 1989.
17. A. Almansa and L. Cohen, "Fingerprint image matching by minimization of a thin-plate energy using a two-step algorithm with auxiliary variables," in *Fifth IEEE Workshop on Applications of Computer Vision*, pp. 35–40, 2000.
18. A. M. Bazen and S. H. Gerez, "Fingerprint matching by thin-plate spline modelling of elastic deformations," *Pattern Recognition* **36**, pp. 1859–1867, August 2003.
19. A. Jain, S. Prabhakar, and A. Ross, "Fingerprint matching: Data acquisition and performance evaluation," Technical Report MSU-CPS-99-14, Michigan State University, March 1999.